Dependence of the Fermi energy upon neutron excess

J.-P. Jeukenne, C. Mahaux, and R. Sartor
University of Liège, Institute of Physics B5, 4000 Liège 1, Belgium
(Received 19 October 1990)

The Fermi energy E_F is defined as the negative of the average between the separation energies of a nucleon from the $(A+1)$- and A-nucleon systems. In the independent-particle limit, E_F is the average between the energies of the last occupied and of the first unoccupied shell-model orbits. For mass numbers $40 \lesssim A \lesssim 208$, the experimental neutron Fermi energies E_{Fn} increase approximately linearly with increasing asymmetry parameter $\eta=(N-Z)/A$. In contrast, the experimental proton Fermi energies E_{Fp} are, on the average, nearly independent of η; when the average single-particle Coulomb energy E_C is subtracted, the quantity $E_{Fp}-E_C$ decreases linearly with increasing η, with a slope whose modulus differs from that found for E_{Fn}. These features are analyzed in the framework of two mean-field models; they both include an isoscalar and an isovector central component, as well as a Coulomb correction in the case of protons. From the comparison between the n-^{208}Pb and p-^{208}Pb mean fields, it is derived that the depth of the symmetry potential is nearly independent of energy in the domain $15 \lesssim E \lesssim 50$ MeV, in close agreement with a recent phenomenological study of the global optical-model potential for nuclei with mass numbers $40 \leq A \leq 208$. In the vicinity of the Fermi energy, the isoscalar and isovector components are assumed to have Woods-Saxon radial shapes and linearly energy-dependent depths. In both models, the depth of the symmetry potential is taken equal to $(23.2-0.46E)$ MeV. In the first model, all the parameters are extracted from a recent dispersion relation analysis of the mean fields felt by neutrons and protons in ^{208}Pb; then, the calculated neutron Fermi energies are in good agreement with the experimental values but the calculated proton Fermi energies are larger than the experimental values, except for the lead isotopes. The second model incorporates, in addition, information derived from dispersion relation analyses of the n-^{40}Ca and n-^{90}Zr potentials; its main characteristics are that the potential radius parameter $r_V=R_V A^{-1/3}$ and the isoscalar depth both depend upon mass number; this second model yields satisfactory agreement with the experimental Fermi energies, not only on the average but also along isotope and isotone chains associated with a magic number of protons or of neutrons. The definition of the isovector potential adopted here is compared with prescriptions used in previous works. Some intrinsic limitations of a mean-field description are pointed out.

I. INTRODUCTION

The experimental determination of the isovector (or symmetry) component of the nuclear mean field faces many problems.[1-3] These are due to the smallness of this component, whose size reaches at most a few percent of the isoscalar strength. They also reflect the difficulty of disentangling the dependence of the mean field upon the mass number A from its dependence upon the asymmetry parameter

$$\eta=(N-Z)/A \ . \tag{1.1}$$

In the case of protons, the existence of a "Coulomb correction" further blurs the empirical analyses. These difficulties can now be efficiently overcome in view of the following recent progress.

(a) An improved phenomenological "global" nucleon optical-model potential has been constructed; here, the word "global" refers to a smooth dependence upon A, η, and the nucleon energy E. This new "CH89" parametrization has been derived by performing optical-model fits to experimental scattering cross sections by targets with mass numbers $40 \leq A \leq 209$, for energies $16 \leq E \leq 65$ MeV in the case of protons and $10 \leq E \leq 26$ MeV in the case of neutrons.[4,5]

(b) In some nuclei, a unified description of the mean field at positive and at negative energies has been achieved by making use of a dispersion relation that connects the real and imaginary parts of the field.[6] The resulting mean field is more accurately determined than in previous phenomenological studies, since it takes into account empirical information at negative as well as at positive energies.

Hence, an improved investigation of the isovector and isoscalar components of the average nucleon-nucleus potential is now feasible. This is the main purpose of the present paper. Our presentation is as follows. In Sec. II, we define the Fermi energy and present a compilation of its empirical values for neutrons and protons in nuclei with mass number $40 \lesssim A \lesssim 208$. Section III contains the basic equations which will be used in the following, and the derivation of the isoscalar and isovector potential depths in ^{208}Pb from recent dispersion relation analyses of the neutron and proton mean fields in ^{208}Pb. In the next three sections, we study to what extent the results obtained in ^{208}Pb account for the main properties of the experimental Fermi energies of other nuclei with

$40 \lesssim A \lesssim 208$. Section IV specifies the quantum numbers of the shell-model orbits adopted in our calculations. In Sec. V, we consider a parametrization which is akin to previous phenomenological analyses in the sense that the potential radius parameter

$$r_V = R_V A^{-1/3} \tag{1.2}$$

is independent of A. Section VI deals with an improved parametrization in which one takes into account the fact that recent analyses indicate that r_V depends upon mass number. Some limitations of a mean-field description are discussed in Sec. VII. In Sec. VIII, we compare the definition of the isovector potential adopted in the present work with those used by other authors. Finally, Sec. IX contains a summary and our conclusions.

II. EXPERIMENTAL FERMI ENERGIES

A. Definition

The separation energy $S_{A\tau}$ of a nucleon from a system with A nucleon is the modulus of

$$E_{F\tau}^{-} = (M_A - M_{A-1} - m_\tau)c^2 , \tag{2.1a}$$

where M_A is the mass of nucleus A, while m_τ denotes the mass of a proton ($\tau = p$) or of a neutron ($\tau = n$). The separation energy of a nucleon from the $(A+1)$-nucleon system is the modulus of

$$E_{F\tau}^{+} = (M_{A+1} - M_A - m_\tau)c^2 . \tag{2.1b}$$

The index τ will be omitted when not necessary. We define the Fermi energy E_F as the average:

$$E_F = \tfrac{1}{2}(E_F^{+} + E_F^{-}) . \tag{2.2}$$

Note that E_F^{-}, E_F^{+}, and E_F are negative quantities. In the independent-particle model, E_F^{-} is identified with the energy of the "last" (least bound) occupied orbit and E_F^{+} with that of the "first" (most bound) unoccupied orbit. This is illustrated in Fig. 1 by the example of neutrons in ^{208}Pb, for which $E_{Fn}^{+} = -3.94$ MeV, $E_{Fn}^{-} = -7.37$ MeV, and $E_{Fn} = -5.65$ MeV. In this section, we perform a compilation of the experimental values of the Fermi energy for neutrons and protons in nuclei with mass numbers $40 \lesssim A \lesssim 208$.

Our motivation for considering the average E_F rather than E_F^{+} or E_F^{-} is the following. The coupling of the single particle to the collective degrees of freedom considerably influences E_F^{+} and E_F^{-} but leaves E_F approximately unchanged.[6] Since this coupling depends upon the specificities of the low-lying excited states of the A-nucleon core, E_F is the quantity that most naturally lends itself to an analysis in the framework of a mean field which depends smoothly upon the quantities A, η, and E. In contrast, a description of both E_F^{+} and E_F^{-} would require a complicated dependence of the potential radius R_V upon energy, besides a dependence upon mass number.

B. Neutron Fermi energies

In the upper part of Fig. 2, we plot experimental values of the neutron Fermi energy versus the asymmetry parameter. We only include even-even nuclei in order to ensure that $E_F^{+} > E_F^{-}$; otherwise theoretical difficulties could exist because the one-body Green's function may have overlapping left-hand and right-hand branch cuts in the complex energy plane.[7] The nuclei with a magic number of neutrons are represented by special symbols because these are the ones which are best suited to a simple mean-field interpretation, as will be discussed in Sec. VII; a linear least-squares fit to the corresponding triangles yields

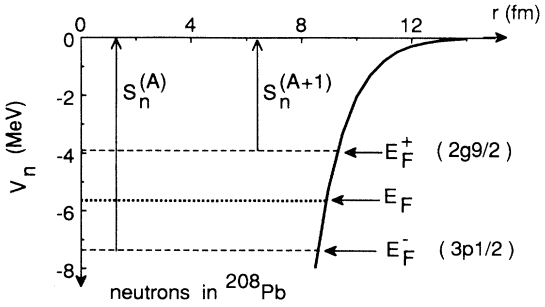

FIG. 1. Illustration of the definition of the quantities E_F^{+}, E_F^{-}, and E_F for neutrons in ^{208}Pb. In the shell-model description, the last occupied subshell is the $3p\frac{1}{2}$ orbit, while the first unoccupied subshell is the $2g\frac{9}{2}$ orbit.

$$E_{Fn} = (-12.52 + 31.3\eta) \text{ MeV} . \tag{2.3a}$$

The experimental value of E_{Fn} are seen to cluster rather closely in the vicinity of this linear parametrization. However, some features indicate that the Fermi energy does not solely depend upon η. For instance, two triangles lie at $\eta = 0.111$ and are separated by 2.44 MeV: they correspond to ^{36}S ($E_{Fn} = -7.14$ MeV) and to ^{90}Zr ($E_{Fn} = -9.58$ MeV).

C. Proton Fermi energies

The lower part of Fig. 2 shows experimental proton Fermi energies. As in the case of neutrons, we use different symbols for nuclei with nonmagic Z than for nuclei with magic Z; a linear least-squares fit to the latter values yields

$$E_{Fp} = (-6.88 - 7.1\eta) \text{ MeV} . \tag{2.3b}$$

The experimental proton Fermi energies show considerable scatter about this linear approximation. In particular, the open symbols fall on nearly parallel lines which tend to intersect the linear approximation (2.3b); each of these lines corresponds to a different isotope chain, as will be discussed in Sec. VI. The comparison between Eqs. (2.3a) and (2.3b) shows that the dependence of the Fermi energy upon η is much weaker for protons than for neutrons. A similar difference exists between the η dependence of the volume integral per nucleon of the optical-model potentials for protons and for neutrons.[1]

We now briefly discuss the Coulomb energy shift and the "Coulomb correction." Let us for simplicity consider an $N = Z$ nucleus. Then, the difference between the pro-

ton and neutron mean fields is due to the fact that a proton feels a Coulomb potential. In the nuclear interior, one can approximate this effect by means of an average "Coulomb energy" E_C given by

$$E_C=(1.73Z/R_C)\ \text{MeV}\ , \tag{2.4a}$$

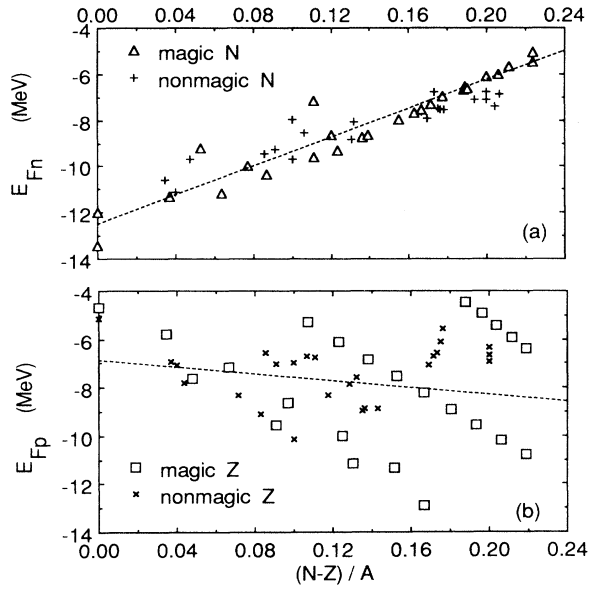

FIG. 2. Dependence upon the asymmetry parameter of experimental Fermi energies, as derived from separation energies compiled in Ref. 8. (a) The upper drawing shows the neutron Fermi energies: the open triangles correspond to nuclei with a magic number of neutrons, namely, $N=20$, (^{40}Ca, ^{38}Ar, and ^{36}S, in order of increasing η), $N=28$, (^{56}Ni, ^{54}Fe, ^{52}Cr, ^{50}Ti, and ^{48}Ca), $N=50$ (^{94}Ru, ^{92}Mo, ^{90}Zr, ^{88}Sr, ^{66}Kr, and ^{84}Se), $N=82$ (^{146}Gd, ^{144}Sm, ^{142}Nd, ^{140}Ce, ^{138}Ba, ^{136}Xe, and ^{134}Te), and $N=126$ (^{214}Ra, ^{212}Rn, ^{210}Po, ^{206}Hg, and ^{208}Pb); in the evaluation of E_F for ^{146}Gd, E_F^- has been associated with the first excited state (at 27.3 keV) in ^{145}Gd because it has the same angular momentum and parity $\frac{3}{2}^+$ as the ground states of the other $N=81$ nuclei of this series of isotones. The dashed straight line represents the linear least-squares fit to the triangles, Eq. (2.3a). The plusses correspond to other even-even nuclei chosen at random, namely (in order of increasing η) ^{36}Ar, ^{58}Ni, ^{50}Cr, ^{42}Ca, ^{70}Ge, ^{44}Ca, ^{40}Ar, ^{80}Kr, ^{94}Mo, ^{46}Ca, ^{106}Pd, ^{120}Sn, ^{130}Xe, ^{150}Sm, ^{160}Dy, ^{170}Yb, ^{180}W, ^{124}Sn, ^{190}Os, ^{200}Hg, ^{206}Pb, and ^{126}Sn. (b) The lower drawing shows proton Fermi energies: the open squares correspond to nuclei with a magic number of protons, namely $Z=20$ (^{40}Ca, ^{42}Ca, ^{44}Ca, ^{46}Ca, and ^{48}Ca), $Z=28$ (^{58}Ni, ^{60}Ni, ^{62}Ni, ^{64}Ni, and ^{66}Ni), $Z=50$ (^{112}Sn, ^{114}Sn, ^{116}Sn, ^{118}Sn, ^{120}Sn, ^{122}Sn, ^{124}Sn, ^{126}Sn, and ^{128}Sn), and $Z=82$ (^{202}Pb, ^{204}Pb, ^{206}Pb, and ^{208}Pb). In five cases (^{48}Ca, ^{122}Sn, ^{124}Sn, ^{126}Sn, and ^{128}Sn), the energies of the first excited states of ^{47}K, ^{123}Sb, ^{125}Sb, ^{127}Sb, and ^{129}Sb were used for evaluating E_{Fp}^- or E_{Fp}^+, in order to retain the same angular momentum and parity for the nuclei of each isotope chain, so that the levels correspond to the same shell-model orbits throughout the chain. The dashed line is the linear least-squares fit to the open symbols, Eq. (2.3b). The crosses correspond to even-even nuclei chosen at random, namely (in order of increasing η) ^{44}Ti, ^{50}Cr, ^{46}Ti, ^{56}Fe, ^{48}Ti, ^{70}Ge, ^{66}Zn, ^{80}Kr, ^{40}Ar, ^{94}Mo, ^{90}Zr, ^{68}Zn, ^{78}Se, ^{106}Pd, ^{74}Ge, ^{88}Sr, ^{84}Kr, ^{130}Xe, ^{140}Ce, ^{150}Sm, ^{160}Dy, ^{170}Yb, ^{200}Hg, ^{180}Hf, and ^{190}Os.

where R_C is the "Coulomb radius" expressed in fm. The depths of the neutron and proton potentials are related by

$$U_p(E+E_C)\approx U_n(E)\quad \text{for } N=Z\ . \tag{2.4b}$$

In that approximation, the difference between the neutron and the proton Fermi energies is approximately equal to E_C. The central values of the proton and neutron effective masses are defined as follows:

$$m_\tau^*/m=1-\frac{d}{dE}U_\tau(E)\ , \tag{2.5}$$

with $\tau=p,n$. By expanding the left-hand side of Eq. (2.4b), one finds

$$U_p(E)\approx U_n(E)+U_C,\quad \text{for } N=Z\ , \tag{2.6a}$$

where

$$U_C=-(1-m_p^*/m)E_C \tag{2.6b}$$

is called the "Coulomb correction."

An empirical method for determining E_C has been proposed by DeVito *et al.*[9,10] These authors derive E_C from the difference between the energies at which the maxima and minima of the proton and neutron elastic-scattering cross sections lie at the same angles. This procedure yields[9,10]

$$E_C(^{40}\text{Ca})=7.0\ \text{MeV}\ , \tag{2.7a}$$

$$E_C(^{208}\text{Pb})=18.8\ \text{MeV}\ ; \tag{2.7b}$$

the uncertainty of these empirical values is about 10%. The estimate (2.7a) is in good agreement with the difference (7.29 MeV) between the proton and neutron Fermi energies in ^{40}Ca. The precise value of E_C is not of much importance in the present context. Henceforth, we shall adopt the following parametrization for the Coulomb radius:

$$R_C=(1.39+1.04A^{1/3})\ \text{fm}\ ; \tag{2.7c}$$

the numerical values of the coefficients on the right-hand side have been determined in order to reproduce the empirical values (2.7a) and (2.7b) of the Coulomb energies in ^{40}Ca and ^{208}Pb. The parametrization (2.7c) is similar to the one used in the CH89 global optical-model potential.[4,5]

Figure 3 gathers the experimental values of the neutron Fermi energy E_{Fn} and of the following "Coulomb-corrected proton Fermi energy:"

$$E_{F,p-C}=E_{Fp}-E_C\ . \tag{2.8a}$$

The latter quantity takes some account of the Coulomb shift implied by Eq. (2.4b); here, we introduce it in order to be able to include in a single drawing an overview of the experimental information on both the neutron and proton Fermi energies. A linear least-squares fit to those experimental values of $E_{F,p-C}$ which are associated with nuclei with magic Z yields

$$E_{F,p-C}=(-11.88-57.5\eta)\ \text{MeV}\ . \tag{2.8b}$$

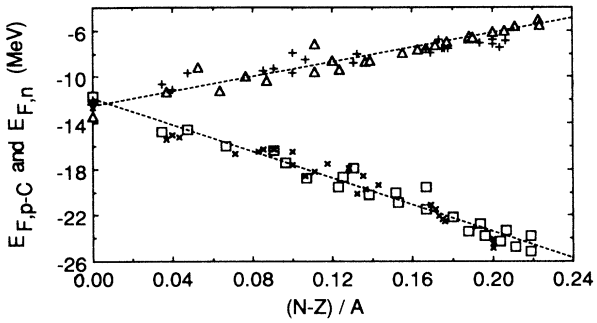

FIG. 3. Dependence upon the asymmetry parameter of the empirical values of neutron and Coulomb-corrected proton Fermi energies [Eq. (2.8a)], with the same notation as in Fig. 2. The dashed lines are linear least-squares fits to the open symbols [Eqs. (2.3a) and (2.8b)].

The experimental values of $E_{F,p-C}$ cluster rather closely about this linear fit. At first sight, this appears to support the often stated property that E_C and η vary "in parallel fashion" along the stability line (Ref. 1, p. 412); however, Fig. 4 exhibits that the latter statement only holds "globally," in particular because E_C is nearly constant along isotope chains.

III. ISOSCALAR AND ISOVECTOR POTENTIAL DEPTHS IN ^{208}Pb

A. Basic equations

For nuclei with $N \neq Z$, the relation (2.4b) must be modified to take into account the existence of a symmetry potential with depth $\pm\eta U_1$, where the $+(-)$ sign corresponds to neutrons (protons). One then has[11]

$$U_n(E+\eta U_1)=U_0(E)+\eta U_1(E) \ . \tag{3.1a}$$

$$U_p(E-\eta U_1+E_C)=U_0(E)-\eta U_1(E) \ . \tag{3.1b}$$

Here, $U_0(E)$ is the depth of the isoscalar potential and $U_1(E)$ that of the isovector potential. By expanding the left-hand sides of Eqs. (3.1a) and (3.1b) and retaining terms up to first order in η and in the energy derivatives, one finds

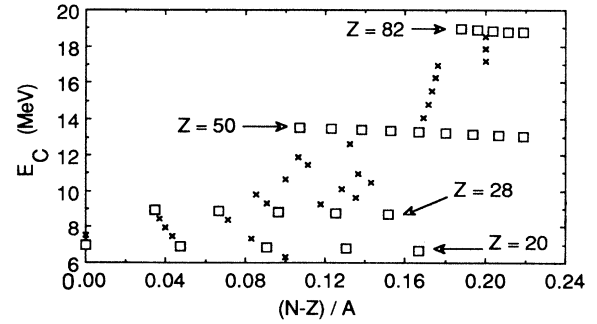

FIG. 4. Plot of the Coulomb energy [Eqs. (2.4a) and (2.7c)] versus the asymmetry parameter, with the same notation as in the lower part of Fig. 2.

$$U_n(E)=U_0(E)+\eta\frac{m_n^*}{m}U_1(E) \ , \tag{3.2a}$$

$$U_p(E)=U_0(E)-\eta\frac{m_p^*}{m}U_1(E)+U_C \ . \tag{3.2b}$$

These relations yield

$$U_0(E)=U_n(E)-\eta\frac{m_n^*}{m}U_1(E) \ , \tag{3.3a}$$

$$U_1(E)=\left[2\eta\frac{m^*}{m}\right]^{-1}[U_n(E)-U_p(E)+U_C] \ , \tag{3.3b}$$

where

$$m^*=\tfrac{1}{2}(m_n^*+m_p^*) \tag{3.3c}$$

is the average effective mass. Above, we do not explicitly refer to a possible energy dependence of the effective masses because we shall approximate the potential depth by linear functions of energy in the vicinity of the Fermi energy: then, the effective masses are independent of energy.

In the vicinity of E_F, the potential radius increases with energy.[6] This energy dependence sizably decreases the particle-hole energy gap $(E_F^+-E_F^-)$; it should thus be taken into account if one wanted to reproduce the values of both E_F^+ and E_F^-. However, it can be neglected if one only wants to reproduce the average of E_F^+ and E_F^- as in the present work. Since we shall omit the energy dependence of the potential radius, we expect to find too large a value for E_F^+ and too small a value for E_F^- as compared to the experimental quantities.

We parametrize all potential shapes by Woods-Saxon form factors. We thus write ($k=p$, n, 1, or 0)

$$V_k(r;E)=U_k(E)f(X_V) \ , \tag{3.4a}$$

$$f(X_V)=(1+\exp X_V)^{-1} \ , \tag{3.4b}$$

$$X_V=(r-R_V)/a_V, \quad R_V=r_V A^{1/3} \ , \tag{3.4c}$$

$$U_k(E)=\alpha_k+\beta_k E \ . \tag{3.4d}$$

The latter linear approximation will only be used in the vicinity of E_F. Equations (3.2a)–(3.3c) yield

$$\beta_n=\frac{\beta_0+\eta\beta_1}{1+\eta\beta_1}, \quad \beta_p=\frac{\beta_0-\eta\beta_1}{1-\eta\beta_1} \ , \tag{3.5a}$$

$$\alpha_n=\alpha_0+\eta(1-\beta_n)\alpha_1 \ , \tag{3.5b}$$

$$\alpha_p=\alpha_0-\eta(1-\beta_p)\alpha_1-\beta_p E_C \ . \tag{3.5c}$$

We shall adopt, for all nuclei, the following typical values for the diffuseness and for the spin-orbit coupling:[12]

$$a_V=0.68 \text{ fm} \ , \tag{3.6a}$$

$$V_{ls}(r)=U_{ls}\frac{1}{r}\frac{d}{dr}f(X_{ls}) \ , \tag{3.6b}$$

$$U_{ls}=11.5 \text{ MeV}, \quad r_{ls}=1.105 \text{ fm}, \quad a_{ls}=0.50 \text{ fm} \ . \tag{3.6c}$$

B. Potential depths in ^{208}Pb

The dispersion relation approach has recently been used[6] to evaluate the average potentials felt by protons and neutrons in ^{208}Pb. In that work, slightly different values were adopted for the proton and neutron radius parameters at the Fermi energy, namely, $r_{Vp}=1.235$ fm and $r_{Vn}=1.225$ fm. Since the difference between these two values is smaller than their uncertainty, we take here

$$r_V=1.23 \text{ fm} . \tag{3.7}$$

Near the Fermi energy, the corresponding potential depths are equal to

$$U_n(E)\approx(-45.78+0.178E) \text{ MeV} , \tag{3.8a}$$

$$U_p(E)\approx(-59.23+0.324E) \text{ MeV} . \tag{3.8b}$$

These depths reproduce the experimental values of the Fermi energies for protons and neutrons in ^{208}Pb. Because of that requirement and of the radius parameter, Eq. (3.7), adopted here, the parametrizations (3.8a) and (3.8b) are slightly different from those given in Ref. 6; this difference also derives from the values adopted here for the diffuseness and for the spin-orbit coupling.

By using Eqs. (3.3a), (3.3b), (3.8a), and (3.8b), one obtains the values of $U_0(E)$ and $U_1(E)$ shown in Fig. 5. These results confirm that the depths $U_0(E)$ and $U_1(E)$ can accurately be approximated by linear functions of energy in the vicinity of the Fermi energy; there, one can write

$$U_0(E)\approx(-49.82+0.258E) \text{ MeV} , \tag{3.8c}$$

$$U_1(E)\approx(23.22-0.461E) \text{ MeV} . \tag{3.8d}$$

The depth of the symmetry potential deviates from the linear approximation (3.8d) for energies larger than 10 MeV. In particular, it presents a plateau ($U_1\approx 15$ MeV)

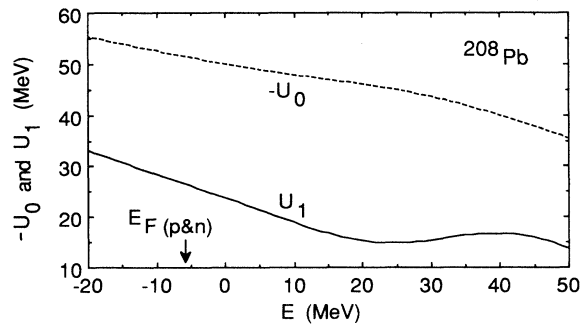

FIG. 5. Energy dependence of the central depth of the symmetry potential and of the absolute value of the depth of the isoscalar potential in ^{208}Pb, as derived from dispersion relation analyses of the neutron- and proton-^{208}Pb mean fields. The neutron and proton potential depths found in Ref. 6 have been slightly readjusted to account for the different values adopted here for the radius parameter, the diffuseness, and the spin-orbit coupling. The arrow points to the value of the Fermi energies for neutrons (-5.65 MeV) and protons (-5.91 MeV); they are too close to be graphically distinguished.

in the energy domain $20\lesssim E\lesssim 50$ MeV. This feature accounts for the phenomenological observation that, in the optical-model analyses of Refs. 4 and 5, no evidence was found of any energy dependence of the symmetry potential in the energy domain $20\lesssim E\lesssim 50$ MeV. In this "CH89" global parametrization, the depth of the phenomenological symmetry potential is $U_t=13.1\pm 0.8$ MeV.

IV. SHELL-MODEL ORBITS

In the next two sections, we shall consider two different mean-field models for calculating the Fermi energies. In order to perform these calculations, one must be able to associate with well-defined shell-model orbits the odd particle or hole in the ground states of the $(A+1)$- and $(A-1)$-nucleon systems. For this main reason, we shall apply these mean-field models to the neutron Fermi energies of nuclei with a magic number of neutrons, and to the proton Fermi energies of nuclei with a magic number of protons. In the case of protons, the average Coulomb field will be identified with the Coulomb potential of a uniformly charged sphere whose radius R_C is given by Eq. (2.7c).

We adopt the following quantum numbers for the shell-model orbits. For N or $Z=20$, we associate F^+ with the $1f_{\frac{7}{2}}$ subshell and F^- with the $(1d_{\frac{3}{2}})^{-1}$ subshell. For N or $Z=28$, we take $F^+=2p_{\frac{3}{2}}$ and $F^-=(1f_{\frac{7}{2}})^{-1}$. For N or $Z=50$, we adopt $F^+=2d_{\frac{5}{2}}$ and $F^-=(1g_{\frac{9}{2}})^{-1}$. For $N=82$, we take $F^+=2f_{\frac{7}{2}}$ and $F^-=(2d_{\frac{3}{2}})^{-1}$, while for $Z=82$ we set $F^+=1h_{\frac{9}{2}}$ and $F^-(3s_{\frac{1}{2}})^{-1}$. Finally, $F^+=2g_{\frac{9}{2}}$ and $F^-=(3p_{\frac{1}{2}})^{-1}$ for $N=126$.

These quantum numbers are in keeping with the measured angular momentum and parity of the relevant ground states, with the following few exceptions. The ground states of $^{A+1}$Sb for $A+1=113$, 115, 117, 119, and 121 have $J^\pi=\frac{5}{2}^+$, in keeping with our $2d_{\frac{5}{2}}$ assignment. However, the ground states of $^{A+1}$Sb for $A+1=123$, 125, 127, and 129 have $J^\pi=\frac{7}{2}^+$; in these cases, we calculated E_F^+ from the first excited state, which has $J^\pi=\frac{5}{2}^+$. For a similar reason, E_F^- for protons in ^{48}Ca has been derived from the first excited state of ^{47}K which has $J^\pi=\frac{3}{2}^+$ in keeping with our $(2d_{\frac{3}{2}})^{-1}$ assignment (the ground state of ^{47}K is a $\frac{1}{2}^+$ level). In the case of neutrons, the sole similar situation is E_F^- in ^{146}Gd, that we derived from the $\frac{1}{2}^+$ first excited state of ^{145}Gd in keeping with our $(3s_{\frac{1}{2}})^{-1}$ assignment.

V. CONSTANT-GEOMETRY MODEL

In most phenomenological investigations of the isovector component of the mean field, it is *a priori* assumed that the quantities U_0, U_1, and r_V are independent of mass number. This is the model considered in the present section. We refer to it as the "constant-geometry model" because one of its main characteristics is that the radius parameter r_V is independent of the mass number A. We determine all the parameters of the model from the dispersion relation analysis of the mean field felt by protons and neutrons in ^{208}Pb; they are fully specified by

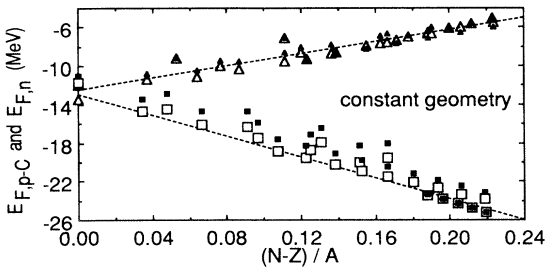

FIG. 6. Dependence upon the asymmetry parameter of the neutron Fermi energies and of the Coulomb-corrected proton Fermi energies [Eq. (2.8a)] for nuclei with a magic number of neutrons or protons. The open symbols represent the same empirical values as in Fig. 3, while the solid symbols have been calculated from the constant-geometry model of Sec. V. The dashed lines are the same as in Fig. 3.

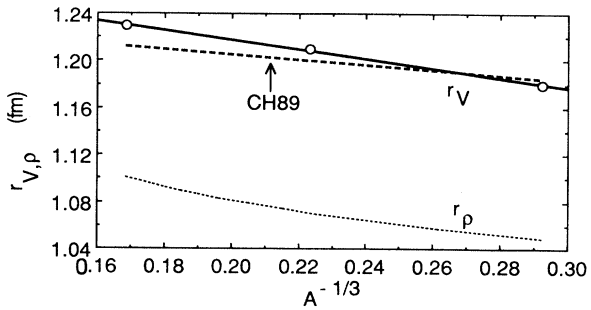

FIG. 7. Dependence upon $A^{-1/3}$ of the radius parameters r_V (associated with the average potential) and r_ρ (associated with the point charge distribution). The open circles give the values of r_V derived from dispersion relation analyses of neutron scattering and bound single-particle data in ^{208}Pb, ^{90}Zr, and ^{40}Ca [Eqs. (6.2a)–(6.2c)]; the solid line represents their parametrization (6.3). The thick dashed line shows the value of r_V in the CH89 global optical-model potential [Eq. (6.1)]. The thin dotted line is the parametrization of r_ρ used by Negele (Refs. 13 and 14).

Eqs. (3.6a)–(3.8d). We calculate the energies E_F^- and E_F^+ of the shell-model orbits specified in Sec. IV, and their average E_F. The results are plotted in Fig. 6. It is seen that the constant-geometry model yields a good agreement with the experimental neutron Fermi energies but that it overestimates the proton Fermi energy, except for the lead isotopes. The fact that the proton Fermi energies are overestimated indicates that the assumptions made in the constant-geometry model are not fully justified. An improved model is considered in the next section.

The agreement between the calculated and experimental Fermi energies in ^{208}Pb is trivial since the potentials have been constructed to achieve it. However, the agreement between calculated and observed proton Fermi energies in ^{202}Pb($\eta=0.188$), ^{204}Pb($\eta=0.196$), ^{206}Pb($\eta=0.204$), and ^{210}Pb($\eta=0.219$) is by no means trivial. Indeed, it supports the accuracy of the symmetry potential given by Eq. (3.8b) in the vicinity of ^{208}Pb and, by the same token, the meaningfulness of the defining equations (3.3a) and (3.3b) for the isoscalar and isovector potential depths.

VI. DISPERSIVE MEAN-FIELD MODEL

A. Motivation

One of the main assumptions of the constant-geometry model is that the radius parameter r_V is independent of the mass number A. This is at variance with the following two recent findings.

(a) In the recent "CH89" global parametrization of the optical-model potential at positive energies, it has been found that the fits to the scattering cross sections are significantly improved if r_V increases with increasing mass number; namely, if one takes[4,5]

$$r_V=(1.25-0.225A^{-1/3})\text{ fm}\ , \tag{6.1}$$

this parametrization is represented by the thick dashed line in Fig. 7.

(b) Dispersion relation analyses of the neutron mean field in ^{40}Ca, ^{90}Zr, and ^{208}Pb led to the following values for the radius parameter at the Fermi energy:

$$r_V(A=208)=1.23\text{ fm} \tag{6.2a}$$

for neutrons in ^{208}Pb (Ref. 6 and present work),

$$r_V(A=90)=1.21\text{ fm} \tag{6.2b}$$

for neutrons in ^{90}Zr (Ref. 15), and

$$r_V(A=40)=1.18\text{ fm} \tag{6.2c}$$

for neutrons in ^{40}Ca (Ref. 16). These results are represented by circles in Fig. 7. They are seen to be in excellent agreement with the parametrization

$$r_V=(1.298-0.405A^{-1/3})\text{ fm}\ , \tag{6.3}$$

which is represented by the solid line in Fig. 7. Equations (6.1) and (6.3) are in qualitative agreement. A quantitative agreement should not be expected since Eq. (6.1) was derived from experimental data in the energy domain $20\lesssim E\lesssim 50$ MeV, while Eq. (6.2) gives the potential radius parameter at the Fermi energy. The decrease of r_V with increasing mass number is in keeping with the decrease of the radius parameter r_ρ associated with the point charge density distribution. This is exhibited in Fig. 7, where the thin dashed line represents the parametrization of r_ρ proposed by Bethe.[13] The difference between r_ρ and r_V is due to the range and to the density dependence of the effective nucleon-nucleon interaction.[17]

B. Isoscalar potential depth

Henceforth, we adopt the parametrization (6.3) for the radius parameter of both the isoscalar and isovector potentials. Since $\eta=0$ for ^{40}Ca, the neutron-^{40}Ca potential is equal to the isoscalar potential $U_0(E)$. In Ref. 16, the following parametrization was found from a dispersion relation analysis:

$$U_0(^{40}\text{Ca})\approx(-53.5+0.44E)\text{ MeV} \tag{6.4a}$$

in the vicinity of the Fermi energy. This result was obtained for a diffuseness $a_V = 0.70$ fm and a spin-orbit coupling slightly different from Eqs. (3.6b) and (3.6c); it furthermore yields $E_{Fn} = -12.16$ MeV instead of the experimental value $E_{Fn} = -12.0$ MeV. We thus slightly modify the parametrization of Ref. 16 and take the following depth, which reproduces the experimental value of E_{Fn} in ^{40}Ca for $r_V = 1.18$ fm and for our choice of the diffuseness and spin-orbit coupling:

$$U_0(^{40}\text{Ca}) = (-51.95 + 0.44E) \text{ MeV} . \quad (6.4b)$$

For the system n-^{90}Zr, the dispersion relation analysis of Ref. 15 yields

$$U_n(^{90}\text{Zr}) = (-52.45 + 0.24E) \text{ MeV} \quad (6.5a)$$

in the vicinity of $E_{Fn} = -9.583$ MeV. For the same reasons as in ^{40}Ca, we modify this value into

$$U_n(^{90}\text{Zr}) = (-50.30 + 0.24E) \text{ MeV} , \quad (6.5b)$$

which reproduces the experimental value of E_{Fn} for $r_V = 1.21$ fm. For the system n-^{208}Pb, the dispersion relation analysis of Ref. 6 yielded

$$U_n(^{208}\text{Pb}) = (-47.1 + 0.223E) \text{ MeV} . \quad (6.6)$$

For the same reasons as above, we replace this approximation by Eq. (3.8a).

For simplicity, we assume that the isovector potential is given by Eq. (3.8d) for all nuclei. Then, Eqs. (3.3a) and (6.5b) yield the following values of U_0:

$$U_0(^{90}\text{Zr}) = (-52.261 + 0.279E) \text{ MeV} . \quad (6.7)$$

Equations (6.4b), (6.7a), and (3.8c) yield $U_0(E) = \alpha_0 + \beta_0 E$ for $A = 40$, 90, and 208. The values of α_0 and β_0 are plotted in Fig. 8; we parametrize them as follows:

$$\alpha_0 = -27.196 - 201.5A^{-1/3} + 399A^{-2/3} , \quad (6.8a)$$

$$\beta_0 = 0.786 - 5.78A^{-1/3} + 15.7A^{-2/3} . \quad (6.8b)$$

These parametrizations are represented by the dashed curves in Fig. 8.

One of the striking features of Eq. (6.8a) is that the isoscalar potential is deeper for ^{40}Ca and ^{90}Zr than for ^{208}Pb. Figure 9 shows that this is in qualitative agreement with the A dependence of the density near the nuclear center; the latter dependence is implied by the decrease of r_ρ with increasing value of A (Fig. 7) if one assumes that the density distribution has a Fermi radial shape.[14] The similarity between the A dependence of α_0 and of ρ_{central} can only be qualitative in view of the density dependence of the effective interaction; note also that the A dependence of $U_0(E)$ depends upon the value of E.

The A dependence of β_0 can in part be ascribed to the A dependence of the central density, since β_0 is expected to decrease with increasing density. It also reflects the influence of the coupling between the single-particle and the collective degrees of freedom; indeed, this coupling gives rise to a decrease of β_0, and this decrease is larger for heavy nuclei because it approximately scales as $A^{1/3}$.

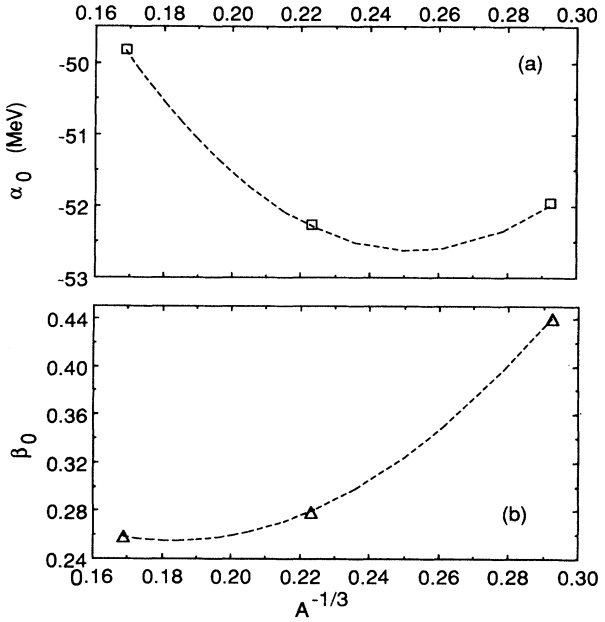

FIG. 8. Dependence of α_0 and β_0 upon $A^{-1/3}$. The open symbols are derived from Eqs. (3.8c), (6.4b), and (6.7a). The dashed curves represent the parametrizations (6.8a) and (6.8b) adopted in the dispersive mean-field model.

C. The model

The "dispersive mean-field model" that we now define differs from the "constant-geometry model" of Sec. V by the following two features. (a) The potential radius parameter depends upon A as described by Eq. (6.3). (b) The depth of the isoscalar potential also depends upon A as specified by Eqs. (6.8a) and (6.8b). For all nuclei, we retain the value of $U_1(E)$ given by Eq. (3.8d), mainly because no empirical information exists on a possible A dependence of U_1; the results shown below support this simplifying assumption.

We recall that the numerical values of the parameters

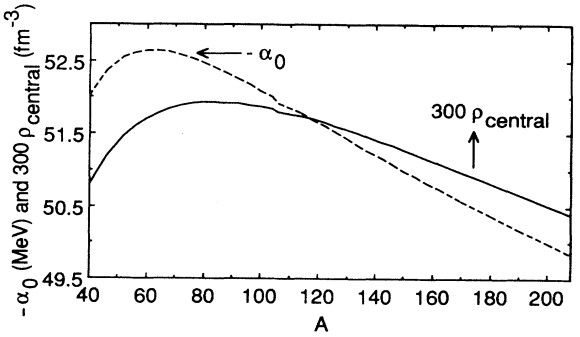

FIG. 9. The dashed curve gives the dependence upon mass number of the absolute value of the depth (in MeV) of the isoscalar potential at zero energy, as parametrized in Eq. (6.8a). The solid curve represents the central density in nuclei as parametrized by Bethe and Negele (Refs. 13 and 14), expressed in units (nucleon/300 fm^3).

which appear in Eqs. (6.3), (6.8a), and (6.8b) have been determined by dispersion relation analyses of the n-^{40}Ca, n-^{90}Zr, and n-^{208}Pb systems; the dispersion relation analysis of the p-^{208}Pb has also been used to derive the symmetry potential $U_1(E)$. Hence, the dispersive mean-field model will, by construction, reproduce the neutron Fermi energies in ^{40}Ca, ^{90}Zr, and ^{208}Pb and the proton Fermi energy in ^{208}Pb. The test of the reliability of the model will thus be provided by the comparison of the other Fermi energies with their experimental values. This comparison is shown in Fig. 10. The overall agreement between the calculated and empirical values is much better than that achieved in the constant-geometry model (Fig. 6). This is remarkable in view of the fact that only four Fermi energies have been fitted, and that the model neglects complications which may arise, for instance, from pairing or from a possible surface peaking of the symmetry potential.

The quality of the agreement between calculated and experimental Fermi energies suggests that a more detailed comparison would be instructive. In Fig. 11, we thus plot the experimental and the calculated values of E_F^+, E_F^-, and E_F for isotope chains associated with magic numbers of protons. The calculated values of E_{Fp}^+ are too large and those of E_{Fp}^- too small; this is due to the fact that a *simple* mean-field model could not reproduce the particle-hole energy gap since the latter is strongly affected by the coupling between the single-particle degree of freedom and the collective low-lying excitations of the surface of the A-nucleon core. Thus, the following discussion only bears on the Fermi energies proper.

Let us first consider the calcium isotopes ($Z=20$). The experimental value of the proton Fermi energy in ^{40}Ca is reproduced within 0.03 MeV, that of ^{48}Ca within 0.06 MeV, and that of ^{46}Ca within 0.20 MeV. This agreement is significant since no proton-calcium data have been used as input in the model; it also puts into better perspective the fact that, in Fig. 10, the calculated values of E_{Fp} are somewhat too large for ^{42}Ca ($\eta=0.048$) and ^{44}Ca ($\eta=0.091$). Indeed, the fact that the calculated E_{Fp} values closely follow the experimental ones along the $Z=20$ chain supports the reliability of the model values for the symmetry potential and for the Coulomb correction. More generally, the fact that the calculated and experimental proton Fermi energies fall on nearly parallel lines for each isotope chain indicates that the strength of the model symmetry potential is reliable.

Figure 12 shows that the difference between the calculated and experimental values of the proton Fermi energies is largest for ^{42}Ca (0.71 MeV) and ^{44}Ca (0.55 MeV); in all the other cases, it is smaller than 0.40 MeV.

In Sec. IV, we pointed out that the angular momentum and parity of the ground and first excited states in the tin isotopes indicate that the energies of the $2d\frac{5}{2}$ and $1g\frac{7}{2}$ "unoccupied" proton orbits cross each other between $A=120$ and $A=122$. Figure 13 shows that this feature is reproduced by our model, although in the latter no parameter has been adjusted to this isotope chain.

Figure 14 shows a detailed comparison between the calculated and experimental values of the neutron Fermi energies. Here again, the agreement is quite satisfactory in view of the simplicity of the model. The least satisfactory case is the $N=82$ chain, for which the difference be-

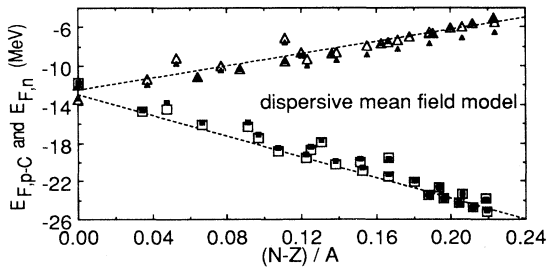

FIG. 10. Dependence upon the asymmetry parameter of the neutron and Coulomb-corrected proton Fermi energies for nuclei with a magic number of neutrons or protons. The open symbols represent the same empirical values as in Fig. 6, while the solid symbols have been calculated from the dispersive mean-field model of Sec. VI. The dashed lines are the same as in Fig. 6.

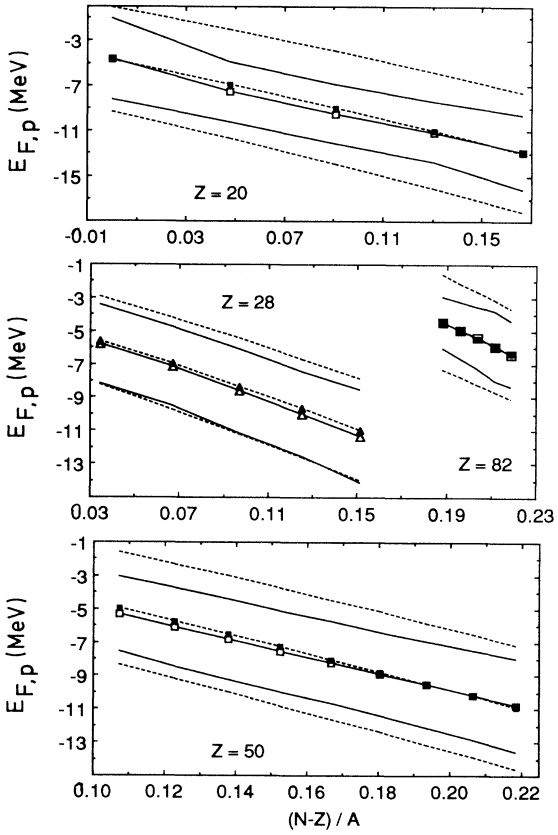

FIG. 11. Dependence of the proton Fermi energies upon the asymmetry parameter, for isotope chains with $Z=20$, 28, 50, and 82. The solid lines connect experimental values of E_F^+, E_F, and E_F^- (from top to bottom); the experimental values of E_F are represented by open symbols. The dashed lines connect the values of E_F^-, E_F, and E_F^+ calculated from the dispersive mean-field model of Sec. VI; the calculated values of E_F are represented by solid symbols.

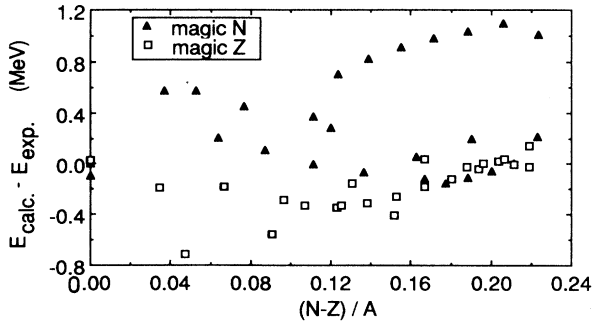

FIG. 12. Difference between the Fermi energies calculated from the dispersive mean-field model and the experimental values. The open squares are associated to protons and the solid triangles to neutrons.

tween calculated and experimental values ranges from 0.71 and 1.10 MeV. This is mainly due to the value of E_{Fn}^{-}. Even in that case, however, the calculated E_{Fn} values run nearly parallel to the experimental values, which confirms that the strength of the model symmetry potential is reliable. We estimate its uncertainty to be about 5 MeV, but a quantitative evaluation of uncertainties in model parameters would require detailed investigations which lie outside the scope of the present study.

Figure 12 shows that the dispersive mean field is, on the average, somewhat too attractive in the case of neutrons and not sufficiently attractive in the case of protons. This could suggest to increase the value of U_1 with decreasing A; one should then also modify the parametrization of $U_0(A)$ as given by Eqs. (6.8a) and (6.8b). We believe that this type of finer adjustment would not be justified in view of the approximations inherent to any mean-field description, as will be outlined in Sec. VII.

D. Components of the neutron and proton potentials

We now discuss some features of the calculated depths of the neutron and proton mean fields and of their components. We display them at the energy -8 MeV, which is typical of the experimental Fermi energies.

The depth of the isoscalar component of the potential is shown in Fig. 15. Because of the dependence of U_0 upon A, the symbols fall on distinct lines. These lines are nearly independent of the asymmetry parameter because nuclei with given magic Z or N have nearly the same mass number. The larger N or $Z \geq 28$ is, the larger A is, and the less deep U_0 is.

Equation (3.2a) expresses the neutron depth $U_n(E)$ as the sum of $U_0(E)$ and of the contribution of the symmetry potential, namely $(\eta m_n^* U_1/m)$. The latter quantity is shown at the top of Fig. 16. The expression (3.2b) of the proton depth is more complicated, since it involves a Coulomb correction U_C besides the contribution $(-\eta m_p^* U_1/m)$ of the symmetry potential; these two contributions are plotted at the bottom of Fig. 16. The Coulomb correction is nearly constant along isotope chains and its absolute value increases with increasing Z, as expected from Fig. 4. For neutrons as well as for protons, the contribution of the symmetry potential lies in the close vicinity of a straight line; the absolute value of the slope of this line is slightly different in the two cases because $m_p^* < m_n^*$ in medium-weight and heavy nuclei.

The depths of the proton and neutron potentials are plotted in Fig. 17. In the case of neutrons, the smooth η dependence of the symmetry contribution maintains the type of structure which exists in the isoscalar depths. In the case of protons, the global increase of U_0 with η is compensated by the increase of the absolute value of the

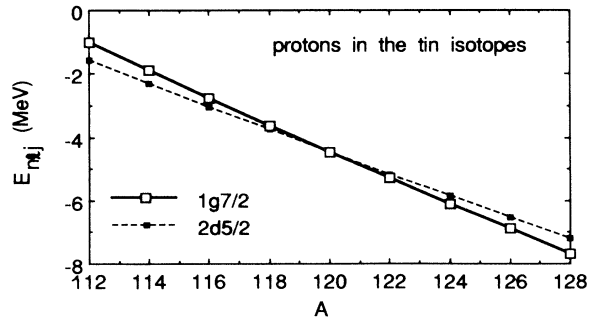

FIG. 13. Dependence upon mass number of the energies of the proton $2d_{\frac{5}{2}}$ and $1g_{\frac{7}{2}}$ orbits in the tin isotopes, as calculated from the dispersive mean-field model.

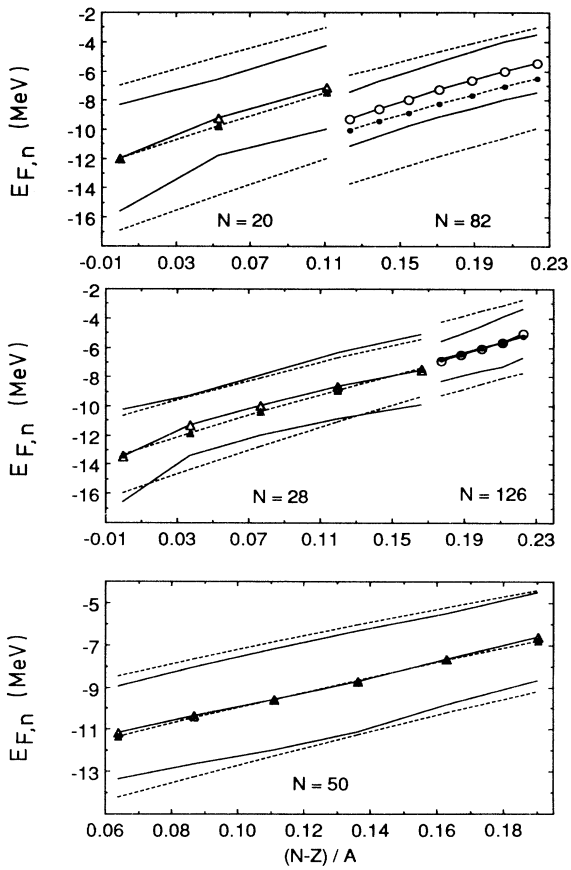

FIG. 14. Same as Fig. 11, for neutron Fermi energies of the isotone chains with $N=20$, 28, 50, 82, and 126.

attractive contributions of the symmetry component and of the Coulomb correction, so that the resulting values of $U_p(E)$ all lie in the close vicinity of a straight line for the nuclei considered here.

E. Fine structure

Perey *et al.*[18,19] performed optical-model fits of the elastic-scattering cross sections of 11 MeV protons by nuclei with $48 \leq A \leq 72$, namely, ^{48}Ti, ^{52}Cr, ^{56}Fe, ^{60}Ni, and ^{64}Zn ($T=2$), ^{49}Ti, ^{51}V, ^{55}Mn, ^{57}Fe, ^{59}Co, and ^{63}Cu ($T=\frac{5}{2}$), ^{58}Fe, ^{62}Ni, ^{66}Zn, and ^{70}Ge ($T=3$), and ^{64}Ni, ^{68}Zn, and ^{72}Ge ($T=4$); here, $T=(N-Z)/2$ denotes the isospin. They found that, if the same geometrical parameters r_V, a_V are adopted in all cases, the phenomenological depths fall close to four different straight lines, each of these being characterized by the value of T. This has been referred to as a "fine structure";[20] it has been argued that it is closely related to a "fine structure" in the experimental values of the Fermi energy.[21] Hence, a brief discussion is of interest in the present context.

The upper part of Fig. 18 shows the proton potential depths at $E=-8$ MeV as calculated from the dispersive mean-field model, for the nuclei investigated by Perey and Perey.[18,19] These depths fall in the vicinity of a straight line, with no visible fine structure. However, one should keep in mind that the model radius parameter r_V depends upon mass number, Eq. (6.3). We now argue that an analysis in terms of an A-independent radius parameter would yield a fine structure. The middle part of Fig. 18 shows the volume integrals per nucleon of the proton potentials, as evaluated from the dispersive mean-field model. It exhibits a fine structure; however, the latter mainly reflects the dependence upon A of the volume integral per nucleon, which is proportional to $(1+x_V^2)$, with $x_V=\pi a_V/R_V$.[1] In order to unravel this factor, we calculate the depths $U_p(E=-8$ MeV) which reproduce the same volume integrals per nucleon as the dispersive mean-field model if one adopts fixed values for the geometrical parameters of all nuclei, namely, $r_V=1.20$ fm and $a_V=0.68$ fm. The results are plotted at the bottom of Fig. 18. It is seen that they exhibit a fine structure. This fine structure is analogous to that found in the phenomenological optical-model fits of Perey *et al.*

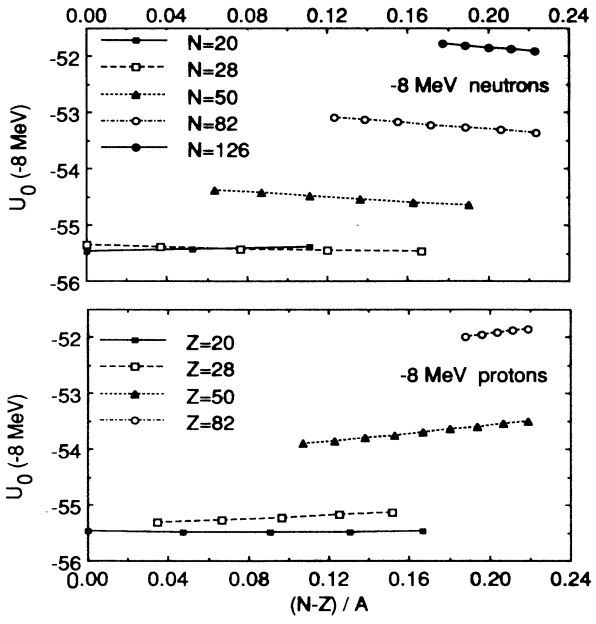

FIG. 15. Dependence upon the asymmetry parameter of the depth of the isoscalar potential for neutrons in nuclei with magic N (top) and for protons in nuclei with magic Z (bottom), as calculated from the dispersive mean-field model. The depths are evaluated at $E=-8$ MeV.

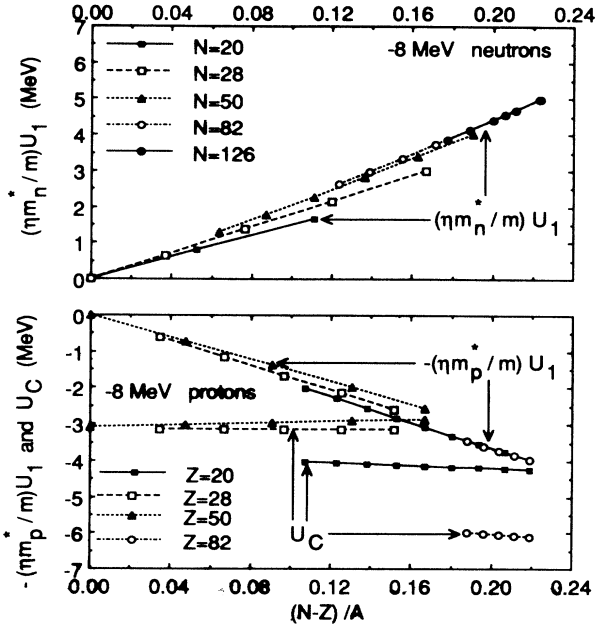

FIG. 16. The upper part shows the contribution of the symmetry component to the neutron potential depths, for nuclei with magic N. The lower part gives the dependence of the contributions of the symmetry component and of the Coulomb correction to the proton potential depth, for nuclei with magic Z. All quantities have been evaluated from the dispersive mean-field model, at $E=-8$ MeV.

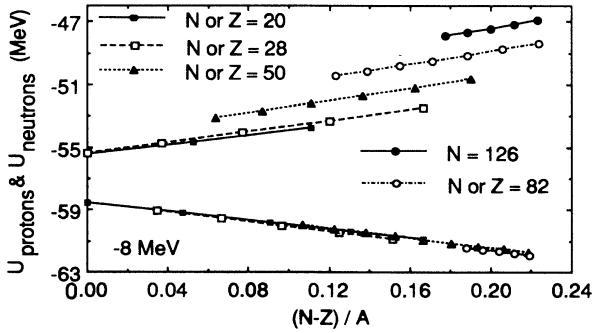

FIG. 17. Depths of the neutron and of the proton potentials, for nuclei with magic N or Z and for $E=-8$ MeV, as evaluated from the dispersive mean-field model.

Indeed, the calculated depths fall on straight lines which are each characterized by a value of T and increase with increasing η. This fine structure is due to the A dependence of the isoscalar component of the mean field, in keeping with an analysis performed in the framework of a nuclear matter calculation with the Reid hard-core nucleon-nucleon interaction.[22] A more quantitative discussion would require the calculation of the Fermi energies E_F. As outlined in the next section, this would involve problems which fall outside the scope of the present work.

VII. LIMITATIONS OF A MEAN-FIELD MODEL

Figures 3 and 4 exhibit that the Fermi energies of nuclei with nonmagic values of N or Z follow the general trend associated with magic values of Z or N. Despite this, the theoretical interpretation of the Fermi energies of nonmagic nuclei requires caution, as had been noticed by Cohen in a pioneering phenomenological study.[23] Let us consider the illustrative example of neutrons in ^{42}Ca.

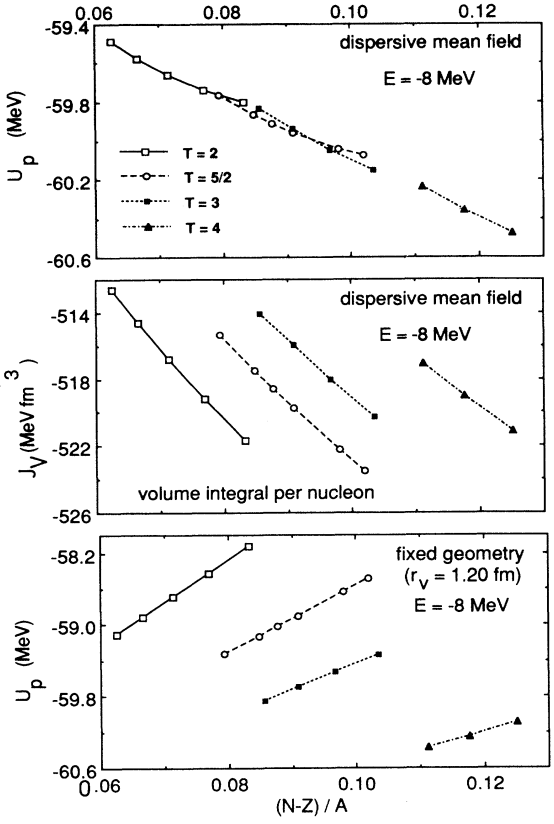

FIG. 18. Depths of the proton potentials at $E=-8$ MeV, for the nuclei investigated by Perey *et al.* (Refs. 18 and 19). The upper drawing contains the depths calculated from the dispersive mean-field model. The middle drawing shows the corresponding volume integrals per nucleon. The lower drawing gives the depths which reproduce the volume integrals per nucleon of the middle drawing when r_V is set equal to 1.20 fm and a_V to 0.68 fm for all nuclei.

The experimental separation energies yield $E_F^+=-7.93$ MeV, $E_F^-=-11.48$ MeV; the corresponding $E_F=-9.71$ MeV is represented by the cross which lies at $\eta=0.048$ in the upper part of Fig. 2. The quantity E_F^- is derived from the separation energy of ^{42}Ca, whose shell-model configuration is $(1f_{\frac{7}{2}})^2$; the quantity E_F^+ is the negative of the separation energy of ^{43}Ca, whose shell-model configuration is $(1f_{\frac{7}{2}})^2(1f_{\frac{7}{2}})$. The difference between the experimental values of E_F^- and E_F^+ thus mainly derives from the pairing energy. The latter is included in a mean-field model in only a global way. Indeed, a mean-field model yields only one $(1f_{\frac{7}{2}})$ orbit and thus one $E_{1f7/2}$ energy. Roughly, this energy corresponds to E_F^+, since the experimental value of E_F^- includes the energy required to break one $(1f_{\frac{7}{2}})^2$ neutron pair. The dispersive mean-field model of Sec. VI yields $E_{1f7/2}=-7.79$ MeV. This is in good agreement with the experimental value of E_F^+ in ^{42}Ca. This agreement is somewhat accidental since the mean-field model is not expected to reproduce E_F^+ or E_F^-. Moreover, a more quantitative reasoning should include the influence of the $(1f_{\frac{7}{2}})^2$ neutron pair in ^{42}Ca on the neutron separation energy of ^{43}Ca. This discussion shows that it would be incorrect to relate the difference $[E_{Fn}(^{42}\mathrm{Ca})-E_{Fn}(^{40}\mathrm{Ca})]$ with the size of the symmetry potential. This remark also applies to the difference $[E_{Fn}(^{40}\mathrm{Ca})-E_{Fn}(^{40}\mathrm{Ar})]$ which has recently been considered in that context.[24]

Pairing effects also influence the separation energy of a neutron from a closed shell. That is the main reason why, in Sec. VI, we mainly considered the Fermi energies associated with isotope or isotone chains with a given magic value of Z or N. Indeed, the Fermi energies of each chain are influenced by pairing in approximately the same way. Nevertheless, one must keep in mind that the size of pairing effects varies from one shell to another. In view of these complications, we believe that it would not be very meaningful to try to improve the agreement reached here between the calculated and experimental values of the Fermi energies.

VIII. COMPARISON WITH OTHER DEFINITIONS OF THE SYMMETRY POTENTIAL

In Ref. 11, the symmetry potential had been defined by Eqs. (3.1a) and (3.1b), which are approximately equivalent to Eqs. (3.2a) and (3.2b). We now briefly discuss the difference with some other definitions.

(a) In many phenomenological analyses, one omits the factors m_n^*/m and m_p^*/m which multiply U_1 on the right-hand side of Eqs. (3.2a) and (3.2b). The "symmetry potential" considered in these analyses should thus be approximately identified with the following quantity:

$$V_t(r;E)\approx\frac{m^*(r;E)}{m}V_1(r;E)\ . \tag{8.1}$$

This remark applies to Refs. 4 and 5. The origin of the factor m^*/m on the right-hand side of Eq. (8.1) was first described in Ref. 25. As discussed in Sec. III B, the value of V_1 found in Refs. 4 and 5 (for positive energies) is in keeping with the present work; it is sizably smaller than

the ones which had been obtained from earlier less complete optical-model analyses.

(b) In Ref. 16, the depth $\tilde{U}_1$ of a "symmetry potential" was derived from the neutron mean field in ^{208}Pb and ^{40}Ca by using the following "prescription:"

$$\eta\tilde{U}_1(E-E_{Fn})=U_n^{208}(E-E_{Fn}^{208})-U_n^{40}(E-E_{Fn}^{40}) , \quad (8.2)$$

where $\eta=0.212$ is the asymmetry parameter of ^{208}Pb. In Ref. 16, the prescription (8.2) was used for the "Hartree-Fock" component of the potential, but this is irrelevant in the present context. The interpretation of the prescription (8.2) is the following: the value of $\tilde{U}_1$ at some energy Δ above the Fermi energy is given by $(\eta)^{-1}$ times the difference between the value of U_n^{208} at the energy $(E_{Fn}^{208}+\Delta)$ and the value of U_n^{40} at the energy $(E_{Fn}^{40}+\Delta)$:

$$\eta\tilde{U}_1(E=E_{Fn}+\Delta)=U_n^{208}(E=E_{Fn}^{208}+\Delta) - U_n^{40}(E=E_{Fn}^{40}+\Delta) . \quad (8.3)$$

By using a linear E-dependence approximation and the notation (3.4d), Eq. (8.3) yields

$$\tilde{U}_1(E=E_{Fn}+\Delta)=\frac{m_n^*}{m}U_1^{208}(E=E_{Fn}^{208}+\Delta) +\eta^{-1}\left[\alpha_0^{208}-\alpha_0^{40}+\Delta\left[\beta_0^{208}-\beta_0^{40}\right] +\beta_0^{208}E_{Fn}^{208}-\beta_0^{40}E_{Fn}^{40}\right] , \quad (8.4)$$

where m_n^* is the neutron effective mass in ^{208}Pb. If one makes the approximations

$$\alpha_0^{40}\approx\alpha_0^{208}, \quad \beta_0^{40}\approx\beta_0^{208} , \quad (8.5)$$

Eq. (8.4) gives

$$\tilde{U}_1(E=E_{Fn}+\Delta)\approx\frac{m_n^*}{m}U_1^{208}(E=E_{Fn}^{208}+\Delta) +\eta^{-1}\beta_0(E_{Fn}^{208}-E_{Fn}^{40}) . \quad (8.6)$$

The second term on the right-hand side of this relation is equal to 10.5 MeV for $\beta_0=0.35$. It approximately cancels the effect of the factor m_n^*/m in the first term. Hence, $\tilde{U}_1(E=E_{Fn}+\Delta)$ would be approximately equal to $U_1^{208}(E=E_{Fn}^{208}+\Delta)$ if the approximations (8.5) would be valid. This was the main motivation for introducing the prescription (8.2) in Ref. 16. In practice, however, the approximations (8.5) are not accurate. Relatedly, the prescription (8.2) yields a result which depends upon the pair of nuclei used in the right-hand side: different results have been obtained from the pair (^{90}Zr,^{40}Ca) and from (^{208}Pb, ^{40}Ca).[15] The main origin of this difficulty lies in the fact that the isoscalar potential depends upon mass number.

IX. SUMMARY AND DISCUSSION

Our main purpose was to investigate the strength of the symmetry potential in the vicinity of the Fermi energy for mass numbers $40\lesssim A\lesssim 208$. In order to be able to use a mean-field approach, the following two main conditions should be fulfilled.

(a) The Fermi energy should not be too sensitive to nuclear structure details. It is for this reason that we defined the Fermi energy as the average between two separation energies (Fig. 1), since this quantity is less influenced than each separation energy by the coupling of the single-particle degree of freedom to the low-lying collective core excitations.

(b) The experimental Fermi energies should have a simple dependence upon the asymmetry parameter. Indeed, a mean field that is a smooth function of N and Z could not yield a complicated dependence upon neutron excess. This second condition is fairly well fulfilled on the average (Fig. 3) although on closer examination the experimental Fermi energies reveal a substructure, which is most conspicuous in the case of protons (Fig. 2).

In order to construct a mean-field model, we made full use of the information on the average potential felt by neutrons and protons in ^{208}Pb recently derived from the dispersion relation approach. The latter presents the advantage of making use of empirical information at both positive and negative energies, thereby yielding mean fields which are more reliable than those constructed from purely phenomenological studies. We derived the depths of the isoscalar and isovector potentials from the n-^{208}Pb and p-^{208}Pb potentials (Fig. 5). While the energy dependence of the isoscalar depth is approximately linear between -20 and $+50$ MeV, it turns out that the isovector depth presents a plateau in the domain $15\lesssim E\lesssim 50$ MeV. This feature is in excellent agreement with the global optical-model parametrization recently deduced from extensive phenomenological optical-model fits of elastic-scattering cross sections by nuclei with mass numbers $40\leq A\leq 208$.[4,5]

In the vicinity of the Fermi energy, the isovector and the isoscalar depths in ^{208}Pb can both be approximated by linear functions of energy [Eqs. (3.8c) and (3.8d)]. We first considered, in Sec. V, a "constant-geometry model" in which these values are adopted for all nuclei, along with the assumption that the potential radius parameter is independent of mass number. This model systematically overestimates the proton Fermi energies, except for the lead isotopes (Fig. 6). Hence, some of the assumptions of the constant geometry are not fully justified. One likely weakness lies in the assumption that the potential radius parameter is independent of mass number. Indeed, recent phenomenological optical-model fits as well as dispersion relation analyses indicate that r_V increases with increasing mass number (Fig. 7). In addition, dispersion relation analyses suggest that the depth of the isoscalar potential also depends upon mass number (Figs. 8 and 9).

In Sec. VI, we thus considered a "dispersive mean-field model" in which the potential radius parameter and the isoscalar depth both depend upon mass number in a way determined by dispersive relation analyses of the n-^{40}Ca, n-^{90}Zr, n-^{208}Pb, and p-^{208}Pb systems. This model yields good agreement with the experimental Fermi energies (Fig. 10). The agreement between calculated and experimental Fermi energies extends to the Fermi energies of each chain of isotopes and isotones with magic values of

Z and N (Figs. 11 and 14). The model also reproduces the crossing of the energies of the $1g_{\frac{7}{2}}$ and $2d_{\frac{5}{2}}$ proton orbits in the tin isotopes (Fig. 13). This detailed agreement has been made possible by the introduction of an A dependence of the isoscalar potential (Fig. 15). This dependence would appear as a "fine structure" in the dependence of the proton depth upon the asymmetry parameter (Fig. 18) if the data were analyzed in terms of a potential with a radius parameter independent of mass number as in the phenomenological optical-model fits performed by Perey *et al.*[18,19]

The comparison between the experimental and calculated Fermi energies has been carried out for nuclei with a magic number of protons or neutrons, because in the independent-particle limit the $(A\pm1)$ systems can then be associated with specific shell-model orbits (Sec. IV). This does not imply that the model is useless in other cases, but caution must then be exercised in the interpretation of the Fermi energy (Sec. VII): indeed, difficulties arise from pairing.

In the study of some nuclear structure problems, e.g., high-spin states, it would be convenient to have at one's disposal a mean field that would reproduce the values of the two separation energies E_F^+ and E_F^- instead of simply their average E_F. This would be more difficult because the dispersion relation approach shows that the potential radius depends upon energy in the vicinity of E_F. This is the main reason why the dispersive mean-field model yields too large values for E_F^+ and too small values for E_F^- (Figs. 11 and 14). It would be conceivable to parametrize the dependence of the radius upon energy as well as upon mass number. However, this would be unduly complicated for most purposes. Indeed, it should often be sufficient to parametrize separately the values of E_F^+ and those of E_F^-, using potential wells which have a larger (A-dependent) radius in the case of E_F^+ than in the case of E_F^-. The resulting single-particle wave functions would still be orthonormal because the valence particle and hole orbits have different angular momentum and/or parity.

Our parametrization of the A dependence of the isoscalar and isovector potentials was based on dispersion relation analyses of only four systems, namely n-^{208}Pb, p-^{208}Pb, n-^{90}Zr, and n-^{40}Ca. It would be of interest to study other systems and to improve the accuracy of the available analyses. For instance, the imaginary part of the mean field was not required to vanish in the energy interval $E_F^- < E < E_F^+$ in the analyses of the n-^{90}Zr and n-^{40}Ca systems as well as in a recent dispersion relation study of the p-^{40}Ca system.[26] A reanalysis of these systems would thus be useful. In particular, it would also be of interest to compare the results derived from the two existing versions of the dispersion relation approach, namely the dispersive optical-model analysis[15,16,26,27] and the variational moment approach.[6,11,28] The latter method has not yet been applied to the n-^{40}Ca, p-^{40}Ca, and n-^{90}Zr systems.

We gratefully acknowledge useful discussions with J. Dudek and C. H. Johnson.

[1]G. R. Satchler, in *Isospin in Nuclear Physics,* edited by D. H. Wilkinson (North-Holland, Amsterdam, 1969), p. 389.
[2]P. E. Hodgson, Nucl. Phys. **A150**, 1 (1970).
[3]J. Rapaport, Phys. Rep. **87**, 25 (1982).
[4]R. L. Varner, T. B. Clegg, T. L. McAbee, and W. J. Thompson, Phys. Lett. B **185**, 6 (1987).
[5]R. L. Varner, W. J. Thompson, T. L. McAbee, E. J. Ludwig, and T. B. Clegg, Phys. Rep. **201**, 57 (1991).
[6]C. Mahaux and R. Sartor, in *Advances in Nuclear Physics,* edited by J. W. Negele and E. Vogt (Plenum, New York, 1991), Vol. 20.
[7]J.-P. Blaizot and G. Ripka, *Quantum Theory of Finite Systems* (MIT, Cambridge, Massachusetts, 1986).
[8]A. H. Wapstra and G. Audi, Nucl. Phys. **A432**, 55 (1985).
[9]R. P. DeVito, S. M. Austin, W. Sterrenburg, and U. E. P. Berg, Phys. Rev. Lett. **47**, 628 (1981).
[10]R. P. DeVito, S. M. Austin, U. E. P. Berg, and W. Sterrenburg, Michigan State University, Report MSUCL-363, 1981 (unpublished).
[11]C. Mahaux and R. Sartor, Nucl. Phys. **A503**, 525 (1989).
[12]J. R. M. Annand, R. W. Finlay, and F. S. Dietrich, Nucl. Phys. **A443**, 249 (1985).
[13]H. A. Bethe (unpublished), quoted on p. 1267 of Ref. 14.
[14]J. W. Negele, Phys. Rev. C **1**, 1260 (1970).
[15]J. P. Delaroche, Y. Wang, and J. Rapaport, Phys. Rev. C **39**, 391 (1989).
[16]C. H. Johnson and C. Mahaux, Phys. Rev. C **38**, 2589 (1988).
[17]J.-P. Jeukenne, A. Lejeune, and C. Mahaux, Phys. Rev. C **16**, 80 (1977); W. J. Thompson, T. L. McAbee, and R. L. Varner, Phys. Lett. B **182**, 247 (1986).
[18]C. M. Perey and F. G. Perey, Phys. Lett. **26B**, 123 (1968).
[19]C. M. Perey, F. G. Perey, J. K. Dickens, and R. J. Silva, Phys. Rev. **175**, 1460 (1968).
[20]P. E. Hodgson, in *Neutron-Nucleus Collisions. A Probe of Nuclear Structure (Burr Oak State Park, Glouster, Ohio),* Proceedings of the Conference of Neutron-Nucleus Collisions—A Probe of Nuclear Structure, edited by J. Rapaport, R. W. Finlay, S. M. Grimes, and F. S. Dietrich, AIP Conf. Proc. No. 124 (AIP, New York, 1985), p. 1.
[21]Y. Wang and J. Rapaport, Nucl. Phys. **A454**, 359 (1986).
[22]M. Jaminon, J.-P. Jeukenne, and C. Mahaux, Phys. Rev. C **34**, 468 (1986).
[23]B. L. Cohen, Am. J. Phys. **33**, 1011 (1965).
[24]C. H. Johnson, R. F. Carlton, and R. R. Winters, ORNL report, 1990 (submitted to Phys. Rev. C).
[25]J. Dabrowski, Phys. Lett. **8**, 90 (1964).
[26]W. Tornow, Z. P. Chen, and J. P. Delaroche, Phys. Rev. C **42**, 693 (1990).
[27]C. H. Johnson, D. J. Horen, and C. Mahaux, Phys. Rev. C **36**, 2252 (1987).
[28]C. Mahaux and R. Sartor, Nucl. Phys. **A493**, 157 (1989).